metals

MDPI

Article

Nanocrystallization in the Duplex Ti-6Al-4V Alloy Processed by Multiple Laser Shock Peening

Wangfan Zhou [1], Xudong Ren [1,*], Fanfan Liu [1], Yunpeng Ren [1] and Lin Li [2,*]

[1] Department of Mechanical Engineering, Jiangsu University, Zhenjiang 212013, China; kinskindom@163.com (W.Z.); jdy.cn@163.com (F.L.); coolim515@163.com (Y.R.)

[2] Laser Processing Research Centre, School of Mechanical, Aerospace and Civil Engineering, The University of Manchester, Manchester M13 9PL, UK

* Correspondence: renxd@mail.ujs.edu.cn (X.R.); lin.li@manchester.ac.uk (L.L.); Tel./Fax: +86-511-8878-0352 (X.R.); +44-0-1612003803 (L.L.)

Academic Editor: Patrice Peyre
Received: 14 October 2016; Accepted: 22 November 2016; Published: 24 November 2016

Abstract: Laser shock peening of titanium alloys has been widely applied in the aerospace industry. However, little is known of the nanocrystalline formation characteristics and mechanisms. In this investigation, a nanocrystalline layer was formed in the duplex Ti-6Al-4V titanium alloy surface region by means of multiple pulsed laser shock peening (LSP). The phase transition and residual stress characteristics of LSP samples were analyzed with X-ray diffraction (XRD) and scanning electron microscopy (SEM). Transmission electron microscopy (TEM) was used to characterize the microstructure and morphologies. As the number of laser pulses increased for each location, higher grain refinement was observed. Micro-hardness testing showed that hardness increased with the number of pulses delivered to each location due to the formation of nanocrystalline layers and high dislocation density in the samples, and a gradient variation of the micro-hardness was obtained. In addition, mechanical twins and different dislocation configurations were formed in the α phase region while only dense dislocation tangles were observed in the β phase region after multiple laser pulse impacts.

Keywords: surface nanocrystallization; laser shock peening; dislocation; titanium alloy

1. Introduction

Titanium alloys have extensive applications in the aerospace and medical industries because of their low density, high strength, and excellent corrosion resistance. However, these alloys always suffer from fatigue loadings in services, and the maximum tensile stress typically locates at the surfaces of the components, which leads to the initiation of the fatigue cracking and early failure. Nanocrystalline metals show excellent mechanical properties, good tribological properties, enhanced electrical resistivity, higher thermal expansion coefficient, and higher heat capacity compared with conventional coarse-grained metals [1–3]. Surface nanocrystallization [4,5] produced by severe plastic deformation (SPD) is the most effective and promising method to induce a nanocrystalline layer in bulk metallic materials and provides a practical approach to improving surface and overall properties of metallic materials. Li et al. [6] fabricated a nanostructured layer with grain sizes in the range of 10–19 nm in the top surface layer of a Ti-6Al-4V alloy by using fast multiple rotation rolling (FMRR) on the surface. Tian et al. [7] performed supersonic Fine Particle Bombarding (SFPB) on a Ti-6Al-4V alloy to form surface structures. They found that the nano-grained surface exhibited a thick nitrogen diffusion layer and high hardness under the same nitriding process. By means of shot peening [8], a gradient nanocrystalline structure with the grain size ranging from the nanometer scale to the micrometer scale was obtained in the bulk coarse-grained TC4 alloy. Bagherifard et al. [9,10] used

severe shot peening (SSP) to process 316L stainless steel. Their results indicated that SSP transformed the austenite phase into a strain-induced α'-martensite in a layered deformation band structure and induced near surface grain refinement to the nano and sub-micron range.

Laser shock peening (LSP) (also called laser peening) is a typical surface treatment method used to extend the fatigue life and improve the mechanical properties of metallic alloys [11–13]. During LSP, metal surfaces experience severe deformation due to the ultra-high strain rate (>10^6 s^{-1}) induced by high-pressure shock waves (on the order of GPa level) and ultra-short pulses (10–30 ns) [14,15]. The investigations on surface nanocrystallization using LSP have attracted wide research interest. Cheng et al. [16] investigated the surface nanocrystallization of a NiTi intermetallic alloy via LSP and found that both strength and ductility are significantly improved through LSP and controlled annealing. A study on the surface nanocrystallization of a TC6 titanium alloy and AISI 304 stainless steel via LSP was conducted by He et al. [17]. They discussed the surface nanocrystallization mechanisms of the two metallic alloys and the effects of different stacking fault energies on surface nanocrystallization. Zhou et al. [18] investigated the surface nanocrystallization and deformation-induced martensite in AISI 304 stainless steel subjected to multiple LSPs. They found that the grain refinement mainly resulted from multidirectional mechanical twins and multidirectional martensite bands during multiple LSP. Our previous work [19] concentrated on the LSP-induced surface nanocrystallization of an AZ91D magnesium alloy and found that surface nanocrystallization was the result of dislocation glide and mechanical twining. However, the investigations of the LSP-induced surface nanocrystallization of the duplex Ti-6Al-4V titanium alloy have been barely reported. The microstructure characteristics of different phases in the duplex Ti-6Al-4V alloy are of importance in understanding the grain refinement and surface nanocrystallization mechanism during LSP. In addition, the effect of LSP parameters on surface nanocrystallization and microstructure evolution in different phases at the subsurface is still unknown.

In this paper, a nanocrystalline layer on the surface of a bulk coarse-grained Ti-6Al-4V titanium alloy was formed via multiple LSP treatments. A systematic investigation on the grain refinement of the LSP-treated Ti-6Al-4V alloy was carried out via X-ray diffraction (XRD), scanning electron microscopy (SEM), and transmission electron microscopy (TEM) analysis. Micro-hardness measurements of the untreated and LSP-treated specimens were carried out, and the reasons for hardness and residual stress improvement are explained. In particular, the microstructure characteristics of different phases in laser peened duplex Ti-6Al-4V alloy are discussed.

2. Material and Experimental Procedure

The nominal chemical composition of the as-received duplex Ti-6Al-4V alloy is shown in Table 1. The Ti-6Al-4V alloy specimens were cut into the dimension of 26 mm × 20 mm× 4 mm (width × length × thickness). All samples were annealed at 760 °C for 2 h and cooled in the air to room temperature before LSP to remove any mechanical machining-induced residual stresses. The samples were ground with silicon carbide paper to grade 1000 and then cleaned in anhydrous alcohol. During laser shock peening, shock waves were induced by a Q-switched Nd:YAG laser system (Thales Laser Ltd., Elancourt, France) operated with a wavelength of 1064 nm and a 10 ns pulse width. The pulse energy used in this experiment was 7.9 J. The laser spot diameter was adjusted to 3 mm on the target surface. An aluminum tape with a thickness of 0.12 mm was used as the absorption layer. The confinement layer to enhance the laser-induced shock wave was running water with a thickness of 3 mm. The detailed parameters of the laser shock experiment are shown in Table 2, and Figure 1 shows the schematic of LSP process.

Table 1. Nominal chemical composition of the Ti-6Al-4V alloy.

Composition	Al	V	C	N	H	O	Ti
Percent (wt %)	5.5–6.8	3.5–4.5	≤0.10	≤0.05	≤0.015	≤0.015	Bal.

Table 2. The parameters used in laser shock peening (LSP).

Parameters	Value
Beam divergence of output (mrad)	≤0.5
Pulse energy (J)	7.9
Spot diameter (mm)	3
Laser pulse width (ns)	10
Laser power intensity (GW/cm^2)	11.2
Repetition-rate (Hz)	5
Overlapping rate (%)	50
Laser wavelength (nm)	1064
Number of laser pulse impacts	1, 3, 5, 7, 10

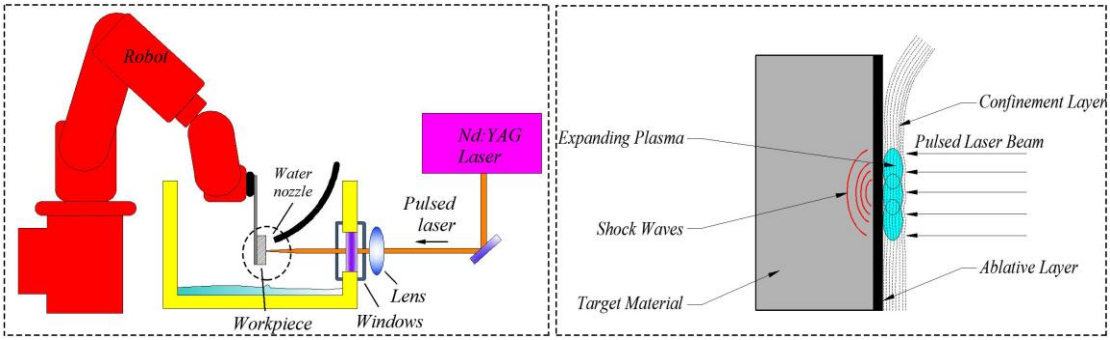

Figure 1. A schematic illustration of LSP.

2.1. Phase Analysis Using XRD

Phase analysis of the Ti-6Al-4V alloy before and after LSP was carried out on a D8 ADVANCE X-ray diffraction (XRD) instrument (Bruker Ltd., Bremen, Germany) with Cu Kα radiation. The diffraction data were collected over a 2θ range of 5°–100°, and the scan speed was 4°/min.

2.2. Measurements of Residual Stress and Micro-Hardness

The depth profiles of the residual stress induced by LSP were measured using XRD with a $\sin^2\psi$ method. The electro-polishing material removal method was used to measure residual stress along the depth and avoid the influence of external stress induced by peeling off material on compressive residual stress. Electro-polishing was performed in a solution of 3.5% saturated sodium chloride solution, and material removal was controlled by the applied voltage and time. The area surrounding the polished region was masked to maintain uniformity and consistency during the material removal. The micro-hardness was measured on the cross sections of the specimens using an HXD-1000TMSC/LCD Micro-hardness tester (Shanghai Optical Instrument Factory, Shanghai, China). The cross sections of the specimens for micro-hardness measurements were prepared via wire-EDM (electro-discharge machining) cutting, and the samples were then subjected to several steps of grinding and polishing. A load of 1.96 N was applied to the micro-hardness measurements with a loading time of 10 s. Micro-hardness results were obtained by taking the average value of 10 different hardness measurements for each sample.

2.3. Microstructure Observations

The microstructures of the original sample were examined via SEM (JEOL Ltd., Tokyo, Japan). Before the SEM, the polished samples were etched using a chemical reagent of 90 mL of H_2O, 8 mL of HNO_3, and 2 mL of HF for 25 s at room temperature. The microstructure evolutions and phases were characterized by a JEM-2100 transmission electron microscope (TEM, JEM-2100, JEOL USA Inc., Pleasanton, CA, USA) operated at a voltage of 200 kV.

3. Results and Discussion

3.1. The Microstructure Prior to LSP

The SEM observation of the duplex Ti-6Al-4V alloy prior to LSP is shown in Figure 2a. The annealed Ti-6Al-4V alloy has a coarse duplex microstructure comprising a primary α phase surrounded by a β phase flake [11,12], as confirmed by the XRD pattern at the upper right corner of Figure 2a. Meanwhile, the primary α phase is mainly featured by its equiaxed morphology. In Figure 2b, the typical bright field (BF) TEM image of the original sample indicates that there are no obvious defects in the primary α and β phases. As shown in Figure 2b, few dislocation lines are observed in the coarse-grained Ti-6Al-4V alloy at the annealed condition.

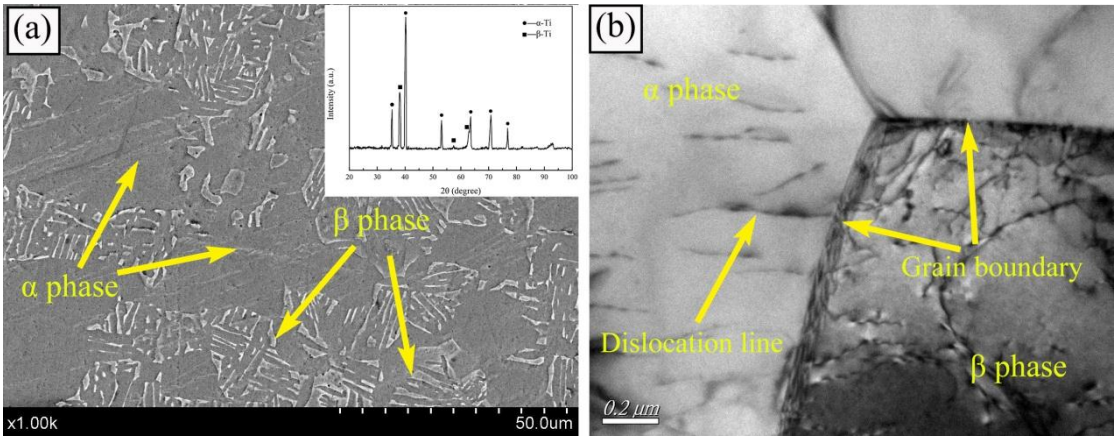

Figure 2. (**a**) The microstructure of the Ti-6Al-4V alloy before LSP and the inset showing the corresponding XRD pattern. (**b**) The bright field TEM image of the coarse-grained alloy.

3.2. XRD Diffraction Phase Analysis

Figure 3a presents the XRD patterns with different LSP impacts. As shown in Figure 3a, there is no additional peak after different LSP impacts, which indicates that no phase transformation occurred and no new crystalline phase was generated, and the main phases are still α and β after laser peening. The severe plastic deformation induced by LSP could result in the increase of microstrain and dislocation density in the material surface, which further contributed to grain refinement. As revealed in the XRD patterns, a dramatic broadening of Bragg diffraction peaks occurred at a different number of impacts, which contributed from grain refinement and the presence of high-level microstrain [20,21].

The Scherrer-Wilson method [22] was used to estimate the average grain sizes and microstrain by analyzing diffraction peaks using the Scherrer-Wilson equation:

$$\mathrm{FW} \times \cos\theta = K \times \lambda / d + 4 \times \varepsilon \times \sin\theta \quad (1)$$

where FW is the broadening of diffraction peaks, K is the shape factor of the lattice constant (1.89), λ is the wavelength of the X-ray radiation (λ = 0.1542 nm), d is the average grain size, ε is the microstrain, and θ is the Bragg angle. As shown in Figure 3b, micro-strain rises, while the grain size decreases with the increase in the number of laser impacts. The grain size reached a sub-micron level when the number of laser pulse impacts exceeds 3. The main reason is that the ultra-high strain rate deformation induced by LSP generates high-density dislocations; moreover, as plastic deformation intensifies, the annihilation and recombination of dislocations lead to the transformation from dislocation walls to grain boundaries, which separates individual grains in the shocked surface. In the next section, more microstructure observations are presented based on transmission electron microscopic analysis to more clearly indicate the microstructure changes near the LSP surface.

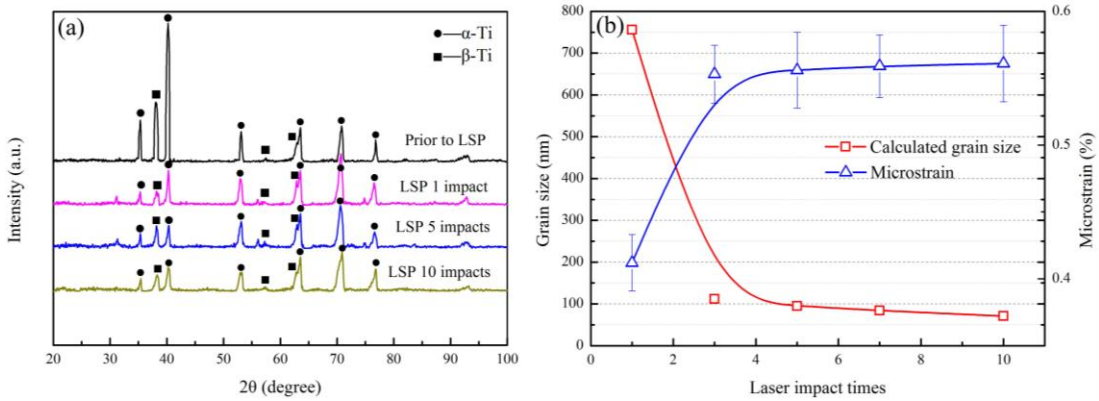

Figure 3. (**a**) The XRD patterns of the Ti-6Al-4V alloy before and after LSP. (**b**) Grain size and micro-strain evolution after the multiple laser peening.

3.3. Nanocrystallization by Multiple LSPs

Figure 4 presents the TEM observation of the LSP-treated surface with different numbers of laser impacts. In Figure 4a, some refined grains with sizes of about 100–150 nm are formed at the top surface, which demonstrates that three LSP impacts are enough to generate nanostructure in the surface region of the Ti-6Al-4V titanium alloy. However, the discontinuous rings in the selected area electron diffraction (SAED) pattern indicate that the distribution of nano-grains is inhomogeneous. The grain sizes become smaller with the number of LSP impacts increasing. With more impacts, the shock wave of the impact continues to generate plastic deformation and refines the grains, which were refined by the anterior impact. However, in Figure 4b,c, the sizes of refined grains are almost in same scale after five and ten impacts, about 80–100 nm. The corresponding SAED pattern illustrated in Figure 4c exhibits nearly complete rings, demonstrating that the nano-grains are random in crystallographic orientation. It illuminates that the relationship between the size of the refined grains and the number of LSP impacts is not linear. The grain refinement becomes saturated after five impacts for the Ti-6Al-4V titanium alloy. This may be ascribed to the upper limit of plastic deformation ability near the material surface. Moreover, the average grain sizes at the treated surface via statistical analysis method are larger than the XRD calculated results, as seen from Figure 4. In fact, the crystal size obtained by the XRD analysis is defined as the size of the coherently scattering domains, which should correspond to the defect-free crystal. Consequently, XRD can distinguish the sub-grains with small misorientations and provide an average size of sub-grains [23], while the conventional TEM observation provides the average size of the grains with high angle grain boundaries.

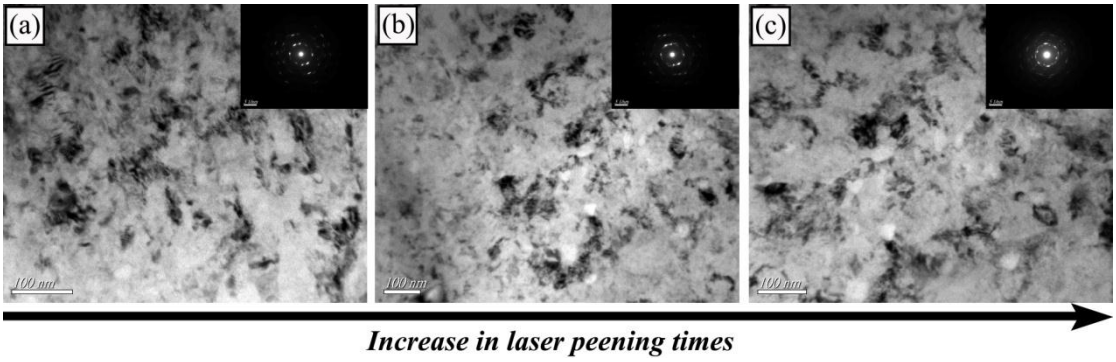

Figure 4. TEM images of nano-grains at the top surface and the inset showing the corresponding SAED patterns. (**a**) 3 LSP impacts; (**b**) 5 LSP impacts; (**c**) 10 LSP impacts.

3.4. Microstructure Characteristics

α and β phases with different atomic arrangements co-exist in the Ti-6Al-4V, and these two phases exhibit different microstructure characteristics during LSP. In Figure 5, TEM images at a depth of about 15–20 μm from the shocked surfaces with different numbers of impacts are presented to understand the microstructure characteristics. Under a single impact, a high density of dislocation tangles was observed in the β phase, while relatively low density was observed in the α phase, as shown in Figure 5a. The β phase with a body-centered cubic (bcc) crystal structure has high stacking fault energy and more slip systems, so dislocation multiplication is easily achieved in this phase. The dislocations in the α phase exhibit regular configuration with distinguishable dislocation lines. Moreover, dislocation walls were formed in the α phase after the single impact, which would further develop toward the sub-grain boundary as plastic deformation intensifies. In Figure 5b, dislocation density in the β phase kept increasing, and some mechanical twins appeared in the α phase after three impacts. The α phase of the Ti-6Al-4V alloy has a hexagonal close-packed (hcp) crystal structure, and only four independent slip systems are available in the α phase. According to the Von-Mises rule, five independent slip systems are necessary to maintain plastic deformation compatibility [24–26]. Therefore, hcp metals usually need other deformations, such as twinning, to accommodate the plastic deformation. Detailed TEM observations in Figure 5c show that high-density twin lamellas with a thickness of several nanometers were formed after five impacts with the laser energy of 7.9 J in the α phase. Furthermore, dense dislocations gathered in the twin boundaries and divided the twins into finer blocks by the twin and dislocation intersections. In Figure 5d, the sub-grain boundaries formed in the α phase after 10 impacts and divided the coarse grains into sub-grains with sizes of 200–300 nm. However, there was still a high density of dislocations inside the sub-grains. The movement of these dislocations were impeded by the phase and grain boundaries, and piled up near these boundaries.

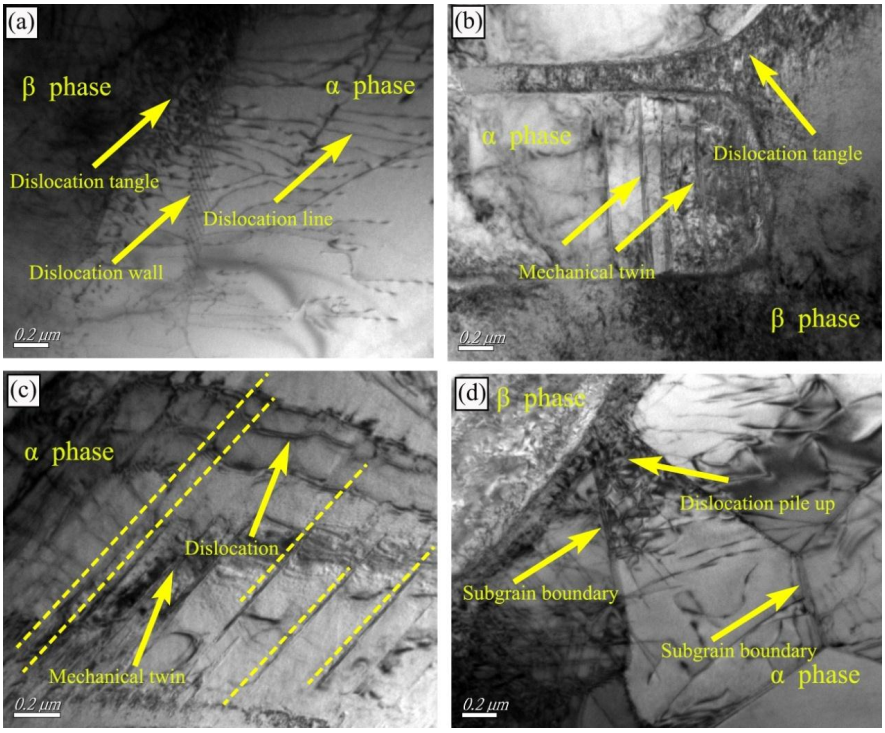

Figure 5. Microstructure characteristics after different numbers of laser pulse impacts. (**a**) Single impact: Parallel dislocation lines are observed in the α phase and high density of dislocation tangles are formed in the β phase. (**b**) 3 impacts: mechanical twins are found in the α phase while dense dislocations in the β phase. (**c**) 5 impacts: plenty of twins are induced in the α phase. (**d**) 10 impacts: a high density of dislocations exists at the grain boundaries and the original coarse grains are divided in to sub-grains.

It is commonly accepted that grain refinement induced by multiple LSP is mainly ascribed to dislocation evolution [18,19,27]. The dislocation evolution involves the development of dislocation lines in the coarse grains, the formation of dislocation tangles and walls due to the dislocation pile up and the transformation of dislocation walls into sub-grain boundaries. The process could be verified by the TEM images. Parallel dislocation lines form after single LSP, and few of them develop into dislocation walls. However, twinning is observed in the α phase after multiple LSP. The interaction between dislocations and twins promote further grain refinement. Twin lamellas divide coarse grains in early deformation, and dislocations subdivide the twins into finer blocks. As the number of impacts increases, dislocation multiplication and movement dominate later refinement.

3.5. Residual Stress and Micro-Hardness Distributions

Material surfaces experienced ultra-high strain rate plastic deformation during LSP, and the severe plastic deformation leads to strain hardening in the treated material, which improves the hardness and residual stresses [27,28]. Figure 6 shows the profiles of the residual stress and micro-hardness on the section with different LSP impacts. As Figure 6 reveals, both compressive residual stress and micro-hardness increased with the number of LSP impacts. For a single impact, the maximum compressive residual stress in the shocked surface was 423 MPa, which grew to 578 and 628 MPa as the number of LSP impacts increased to 5 and 10, respectively, as presented in Figure 6a. The results also indicate that increasing the number of LSP impacts cannot infinitely improve the compressive residual stress at the shocked surface. Moreover, the affected layer, beyond which residual tensile stress will replace compressive stress, was effectively deepened by multiple LSPs. The introduction of the compressive residual stress was the result of dense dislocation structures induced by the LSP as observed in TEM graphs. The surface micro-hardness increased from 331 HV to 415 HV with a single LSP impact, improved by approximately 20%. However, the micro-hardness was just 439 HV with 10 LSP impacts, which indicates that increasing the number of LSP impacts has little improvement on the surface hardness. The hardness improvement is mainly ascribed to the high dislocation density and grain refinement induced by LSP. According the dislocation reinforcement theory, high-density dislocations prevent the generation and movement of other dislocations during plastic deformation; thus, micro-hardness is improved. The Hall-Petch theory [29] illustrates that the yield stress σ_s is linear with $d^{-1/2}$:

$$\sigma_s = \sigma_0 + k \times d^{-1/2} \quad (2)$$

where σ_0 is material constant, k is the slope of Hall-Petch relation curve, and d is the average grain size. The strength and hardness are both improved with grain refinement. The grain size cannot be further refined with 5 or 10 LSP impacts according to the TEM observations, so the improved amplitude of hardness is limited. The hardness decreases with depth, and there is a severe hardening layer about 400 μm along the section after a single impact. The micro-hardness decreased sharply in the shallow layer due to ultra-refined grains in the severe hardening layer. In deep layer, the gradually decreasing hardness is attributed to dislocations, which are caused by the low amplitude pressure of attenuated shock wave. Although increasing LSP impact numbers cannot obviously improve the surface hardness, the affected depth of hardness can be effectively increased. The affected depth of hardness increases from 400 μm for 1 LSP impact to 800 μm for 10 impacts. The increase of the effecting layer depth is ascribed to more time and energy for dislocation and other crystal defect reaction in depth provided by multiple LSP. The LSP-induced deep work hardened surface layer with high compressive residual stresses extends the fatigue life of the material under cyclic loading by inhibiting both fatigue crack initiation and propagation rates.

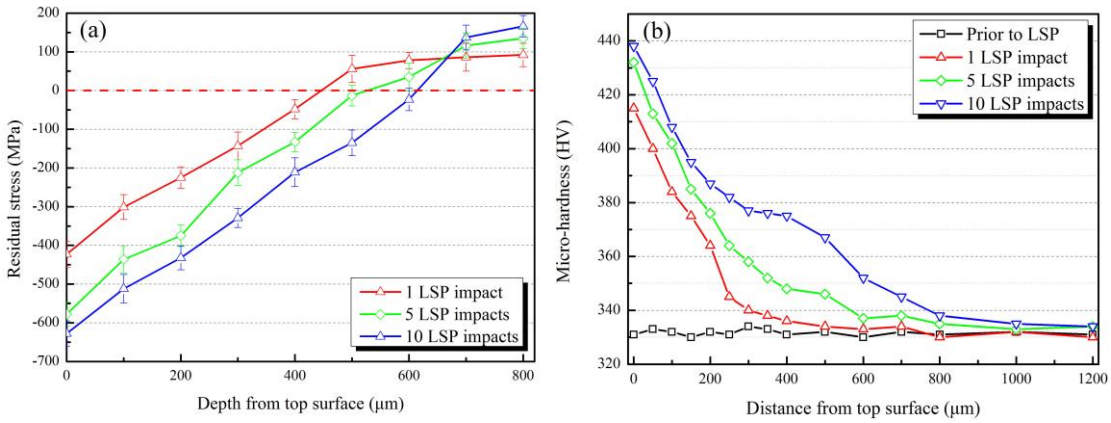

Figure 6. (**a**) Residual stress and (**b**) micro-hardness distribution on cross section with different LSP impacts.

4. Conclusions

In this paper, LSP was performed on the Ti-6Al-4V titanium alloy samples with different numbers of impacts. The following conclusions can be drawn from this work:

(1) There is no distinguishable phase transition after multiple LSP through analyzing the surface XRD patterns. The peak broadening indicates dislocation multiplication and grain refinement induced by LSP.

(2) Nano-grains with diameters of 80–100 nm were formed in the shocked surface after five impacts. The increase of laser pulse impacts has little effect on further grain refinement. However, a higher number of impacts would make the distribution of nano-grains more homogeneous. Regular dislocation lines in the α phase and dense dislocation tangles in the β phase are observed in the subsurface after a single laser impact. After five impacts, mechanical twins are formed in the α phase. The interaction between twins and dislocations become notable.

(3) The micro-hardness and residual stresses exhibit a gradient distribution in the depth direction, and increase with the number of laser pulse impacts due to high dislocation density and grain refinement induced by LSP. The improvements of residual stress and hardness are limited for multiple LSPs, while the number of laser pulse impacts could efficiently deepen the affected layer.

Acknowledgments: The authors are grateful to the project supported by the National Natural Science Foundation of China (Grant Nos. 51611130207, 51479082 and 51275556), the Natural Science Foundation of Jiangsu Province (Grant Nos. BK20160014), the 2015 Innovation & Entrepreneurship Project of Jiangsu Province, the project supported by the Science & Technology Promotion Plan of Ministry of Water Resources of China (Grant No. TG1521), and the Research Innovation Program for College Graduates of Jiangsu Province (Grant No. KYZZ16_0331).

Author Contributions: Xudong Ren conceived and designed the experiments; Fanfan Liu performed the experiments; Wangfan Zhou and Yunpeng Ren analyzed the data; Xudong Ren contributed reagents/materials/analysis tools; Wangfan Zhou wrote the paper; Lin Li reviewed and edited the manuscript and recommended several technical work improvements.

Conflicts of Interest: The authors declare no conflict of interest.

References

1. Yu, H.; Tieu, A.K.; Lu, C.; Liu, X.; Liu, M.; Godbole, A.; Kong, C.; Qin, Q. A new insight into ductile fracture of ultrafine-grained Al-Mg alloys. *Sci. Rep.* **2015**, *5*, 9568. [CrossRef] [PubMed]
2. Valiev, R.Z. Nanostructuring of metals by severe plastic deformation for advanced properties. *Nat. Mater.* **2004**, *3*, 511–516. [CrossRef] [PubMed]

3. Valiev, R.Z.; Islamgaliev, R.V.; Alexandrov, I.V. Bulk nanostructured materials from severe plastic deformation. *Prog. Mater. Sci.* **2000**, *45*, 103–189. [CrossRef]
4. Lu, K.; Lu, J. Surface nanocrystallization (SNC) of metallic materials presentation of the concept behind a new approach. *J. Mater. Sci. Technol.* **1999**, *15*, 193–197.
5. Gangaraj, S.M.H.; Choa, K.S.; Voigt, H.-J.L.; Guagliano, M.; Schuh, C.A. Experimental assessment and simulation of surface nanocrystallization by severe shot peening. *Acta Mater.* **2015**, *97*, 105–115. [CrossRef]
6. Li, Y.; Sun, K.; Liu, P.; Liu, Y.; Chui, P. Surface nanocrystallization induced by fast multiple rotation rolling on Ti-6Al-4V and its effect on microstructure and properties. *Vacuum* **2014**, *101*, 102–106. [CrossRef]
7. Ge, L.; Tian, N.; Lu, Z.; You, C. Influence of the surface nanocrystallization on the gas nitriding of Ti-6Al-4V alloy. *Appl. Surf. Sci.* **2013**, *286*, 412–416. [CrossRef]
8. Liu, Y.G.; Li, M.Q.; Liu, H.J. Surface nanocrystallization and gradient structure developed in the bulk TC4 alloy processed by shot peening. *J. Alloy. Compd.* **2016**, *685*, 186–193. [CrossRef]
9. Bagherifard, S.; Hickey, D.J.; de Luca, A.C.; Malheiro, V.N.; Markaki, A.E.; Guagliano, M.; Webster, T.J. The influence of nanostructured features on bacterial adhesion and bone cell functions on severely shot peened 316L stainless steel. *Biomaterials* **2015**, *73*, 185–197. [CrossRef] [PubMed]
10. Bagherifard, S.; Slawik, S.; Pariente, I.F.; Pauly, C.; Mücklich, F.; Guagliano, M. Nanoscale surface modification of AISI 316L stainless steel by severe shot peening. *Mater. Des.* **2016**, *102*, 68–77. [CrossRef]
11. Spanrad, S.; Tong, J. Characterization of foreign object damage (FOD) and early fatigue crack growth in laser shock peened Ti-6Al-4V aerofoil specimens. *Mater. Sci. Eng. A* **2011**, *528*, 2128–2136. [CrossRef]
12. Srinivasan, S.; Garcia, D.B.; Gean, M.C.; Murthy, H.; Farris, T.N. Fretting fatigue of laser shock peened Ti-6Al-4V. *Tribol. Int.* **2009**, *42*, 1324–1329. [CrossRef]
13. Montross, C.S.; Wei, T.; Ye, L.; Clark, G.; Mai, Y.W. Laser shock processing and its effects on microstructure and properties of metal alloys: A review. *Int. J. Fatigue* **2002**, *24*, 1021–1036. [CrossRef]
14. Ichiyanagi, K.; Nakamura, K. Structural Dynamics of Materials under Shock Compression Investigated with Synchrotron Radiation. *Metals* **2016**, *6*, 17. [CrossRef]
15. Petronic, S.; Sibalija, T.; Burzic, M.; Polic, S.; Colic, K.; Milovanovic, D. Picosecond Laser Shock Peening of Nimonic 263 at 1064 nm and 532 nm Wavelength. *Metals* **2016**, *6*, 41. [CrossRef]
16. Ye, C.; Suslov, S.; Fei, X.; Cheng, G.J. Bimodal nanocrystallization of NiTi shape memory alloy by laser shock peening and post-deformation annealing. *Acta Mater.* **2011**, *59*, 7219–7227. [CrossRef]
17. Lou, S.; Li, Y.; Zhou, L.; Nie, X.; He, G.; Li, Y.; He, W. Surface nanocrystallization of metallic alloys with different stacking fault energy induced by laser shock processing. *Mater. Des.* **2016**, *104*, 320–326. [CrossRef]
18. Zhou, L.; He, W.; Luo, S.; Long, C.; Wang, C.; Nie, X.; He, G.; Shen, X.; Li, Y. Laser shock peening induced surface nanocrystallization and martensite transformation in austenitic stainless steel. *J. Alloy. Compd.* **2016**, *655*, 66–70. [CrossRef]
19. Ren, X.D.; Huang, J.J.; Zhou, W.F.; Xu, S.D.; Liu, F.F. Surface nano-crystallization of AZ91D magnesium alloy induced by laser shock processing. *Mater. Des.* **2015**, *86*, 421–426. [CrossRef]
20. Huang, R.; Han, Y. Structure evolution and thermal stability of SMAT-derived nanograined layer on Ti-25Nb-3Mo-3Zr-2Sn alloy at elevated temperatures. *J. Alloy. Compd.* **2013**, *554*, 1–11. [CrossRef]
21. Li, W.; Liu, P.; Ma, F.C.; Liu, X.K.; Rong, Y.H. High-temperature surface alloying of nanocrystalline nickel produced by surface mechanical attrition treatment. *J. Alloy. Compd.* **2011**, *509*, 518–522. [CrossRef]
22. Williamson, G.K.; Hall, W.H. X-ray line broadening from filed aluminium and wolfram. *Acta Metall.* **1953**, *1*, 22–31. [CrossRef]
23. Khoshkhoo, M.S.; Scudino, S.; Thomas, J.; Gemming, T.; Wendrock, H.; Eckert, J. Size evaluation of nanostructured materials. *Mater. Lett.* **2013**, *108*, 343–345. [CrossRef]
24. Sun, J.L.; Trimby, P.W.; Si, X.; Liao, X.Z.; Tao, N.R.; Wang, J.T. Nano twins in ultrafine-grained Ti processed by dynamic plastic deformation. *Scr. Mater.* **2013**, *68*, 475–478. [CrossRef]
25. Wu, X.L.; Youssef, K.M.; Koch, C.C.; Mathaudhu, S.N.; Kecskes, L.J.; Zhu, Y.T. Deformation twinning in a nanocrystalline hcp Mg alloy. *Scr. Mater.* **2011**, *64*, 213–216. [CrossRef]
26. Liu, H.X.; Hu, Y.; Wang, X.; Shen, Z.B.; Li, P.; Gu, C.X.; Liu, H.; Du, D.Z.; Guo, C. Grain refinement progress of pure titanium during laser shock forming (LSF) and mechanical property characterizations with nanoindentation. *Mater. Sci. Eng. A* **2013**, *564*, 13–21. [CrossRef]

27. Shadangi, Y.; Chattopadhyay, K.; Rai, S.B.; Singh, V. Effect of LASER shock peening on microstructure, mechanical properties and corrosion behavior of interstitial free steel. *Surf. Coat. Technol.* **2015**, *280*, 216–224. [CrossRef]
28. Ren, X.D.; Zhou, W.F.; Ren, Y.P.; Xu, S.D.; Liu, F.F.; Yuan, S.Q.; Ren, N.F.; Huang, J.J. Dislocation evolution and properties enhancement of GH2036 by laser shock processing: Dislocation dynamics simulation and experiment. *Mater. Sci. Eng. A* **2016**, *654*, 184–192. [CrossRef]
29. Nie, X.; He, W.; Zhou, L.; Li, Q.; Wang, X. Experiment investigation of laser shock peening on TC6 titanium alloy to improve high cycle fatigue performance. *Mater. Sci. Eng. A* **2014**, *594*, 161–167. [CrossRef]

© 2016 by the authors; licensee MDPI, Basel, Switzerland. This article is an open access article distributed under the terms and conditions of the Creative Commons Attribution (CC-BY) license (http://creativecommons.org/licenses/by/4.0/).